Journal of Archaeological Science 173 (2025) 106123

Contents lists available at ScienceDirect

Journal of Archaeological Science

journal homepage: www.elsevier.com/locate/jas

Virtual sampling: Archaeological implications of a new technique for elemental mapping of Mg/Ca ratios in marine mollusc shells

Jesús Mirapeix [a,e], Rosa Arniz-Mateos [b,c], Asier García-Escárzaga [d], Igor Gutierrez-Zugasti [c], José Miguel López-Higuera [a,e], Adolfo Cobo [a,c,e,*]

[a] Photonics Engineering Group, Universidad de Cantabria, Santander, Spain
[b] Leibniz Zentrum für Archäologie (LEIZA), Mainz, Rhineland-Palatinate, Germany
[c] Instituto Internacional de Investigaciones Prehistóricas de Cantabria (Universidad de Cantabria, Gobierno de Cantabria, Grupo Santander), Santander, Spain
[d] Department of Prehistory and Institute of Environmental Science and Technology (ICTA), Universitat Autònoma de Barcelona, Bellaterra, Spain
[e] CIBER de Bioingeniería, Biomateriales y Nanomedicina (CIBER-BBN), Instituto de Salud Carlos III, Madrid, 28029, Spain

ARTICLE INFO

Keywords:
Archaeology
Mollusc shells
Season of collection
Elemental ratios
LIBS

ABSTRACT

Marine mollusc shells hold significant potential for deciphering past environmental conditions and seasonality of hominin subsistence strategies. While stable oxygen isotope ratio values of shells are currently the gold standard, they have significant drawbacks, such as complex and time-consuming sampling procedures and assumptions on the oxygen isotope composition of seawater in the past. The analysis of shell elemental ratios offers an alternative with minimal sample preparation and no assumptions on water composition. Although elemental ratios have already shown a correlation with seawater temperatures, this relationship is also influenced by other environmental factors and endogenous physiological mechanisms, resulting in noisy ratio profiles that are dependent on the exact measurement path across the growth lines of the shell. This study introduces "virtual sampling" (VS), a novel technique enhancing the analysis of the Mg/Ca ratios of marine mollusc shells measured by Laser-Induced Breakdown Spectroscopy (LIBS). It is based on the automatic detection of the isochronous -growth- lines and its employment for averaging the elemental ratios. This approach mitigates the noise inherent to linear scanning trajectories and improves the estimation accuracy of the elemental ratios. Our investigation focuses on analysing twenty-four modern and six archaeological *Patella vulgata* Linnaeus, 1758 shells and the effects derived from the application of this virtual sampling versus the traditional techniques. This advancement in elemental analysis provides a more robust basis for seasonal mollusc collection estimations than the linear LIBS scanning and analysis approach, contributing to a better understanding of human lifeways in archaeological studies.

1. Introduction

Deciphering the subsistence strategies developed by past human populations is critical to understanding how our ancestors survived and managed available resources during Prehistory, and the climatic impact on the decision of these strategies. Hominins consumed shellfish at least 250,000 years ago (Ramos-Muñoz et al., 2016; Cortés-Sánchez et al., 2019). However, this food supply was not intensively exploited until the Early Holocene, when marine molluscs played an essential role in the subsistence strategies of human populations inhabiting littoral locations around the world (Jackson et al., 2012; Lewis et al., 2020; Roberts et al., 2020). The increase in intertidal exploitation patterns provoked high accumulations of the non-edible part of the mollusc in the archaeological sites, forming the so-called shell middens all around the world (Colonese et al., 2011; Gutiérrez-Zugasti et al., 2011; Lombardo et al., 2013; Hausmann and Meredith-Williams, 2017).

Considering the importance these resources reached for prehistoric groups, inferring the seasonality of mollusc consumption is a crucial issue for revealing the role played by shellfish in the annual scheduling of human subsistence strategies (Andrus, 2011; Thomas, 2015). To determine the season(s) when the molluscs were harvested, stable oxygen isotope analyses or sclerochronological analyses have traditionally been carried out on subfossil shells (Colonese et al., 2018; García-Escárzaga et al., 2019, 2024a). Stable oxygen isotope ratio ($\delta^{18}O$) values derived from ancient shells can act as a very powerful recorder of the seawater temperatures experienced by the shells throughout the year

* Corresponding author. Photonics Engineering Group, Universidad de Cantabria, Santander, Spain.
E-mail address: adolfo.cobo@unican.es (A. Cobo).

https://doi.org/10.1016/j.jas.2024.106123
Received 15 April 2024; Received in revised form 19 November 2024; Accepted 20 November 2024
Available online 23 November 2024

(Ferguson et al., 2011; Wanamaker et al., 2008b; Flores and Broitman, 2021; García-Escárzaga et al., 2022), thus offering us the possibility of reconstructing i) the climate conditions during the molluscs' lifespan and ii) the season of the year when they died (i.e., when they were collected), and therefore, of deducing the seasonality of littoral resource exploitation strategies of prehistoric human groups (Leng and Lewis, 2016; Colonese et al., 2009; Mannino et al., 2011; Prendergast et al., 2016; García-Escárzaga et al., 2019).

Stable oxygen isotope analyses have been extensively and successfully applied to shells recovered worldwide, providing valuable information in climate and archaeological investigations. However, this methodological approach faces some issues, such as an unknown isotopic composition of the water ($\delta^{18}O_{water}$) in the past that is necessary for the calculation of seawater temperatures (Grossman and Ku, 1986), but not strictly required to estimate the season of collection and expensive and time-consuming sampling and analytical procedures (Andrus, 2011). Regarding the first issue, some works (Gutiérrez-Zugasti et al., 2015) have analysed the impact of seawater composition in the resulting temperatures from ($\delta^{18}O_{shell}$) obtained via the empirical equation proposed by Grossman and Ku (1986). To overcome these inherent limitations of isotopic analyses, efforts have been made to develop independent climate indicators, with trace elements (e.g., magnesium or strontium) being among the most studied.

The variations in elemental ratios (such as Mg/Ca, Sr/Ca or Ba/Ca) also offer insights into past marine environments, as the influence of seawater surface temperature (SST) in the substitution rate of those elements, albeit complex, has been established (Schöne et al., 2019; Brosset et al., 2023; Wanamaker Jr. et al., 2008; Poulain et al., 2015). This relationship also enables the estimation of the season of collection of archaeological samples by looking at the relative variations of the ratio profile in the region close to the shell edge. However, while many studies have shown a robust dependence of the elemental ratios with the SST (Ferguson et al., 2011; Freitas et al., 2012; Cobo et al., 2017; Durham et al., 2017; Prendergast et al., 2017; García-Escárzaga et al., 2021), many others have shown heterogeneous results in some species (Freitas et al., 2005; Wanamaker et al., 2008b; Schöne et al., 2011; Poulain et al., 2015; Marali et al., 2017). Environmental or physiological factors such as ontogeny, stressors, metabolism, growth rate variations, food resources, or water salinity could affect the incorporation of trace elements and seem to be very species-specific (Schöne, 2008; Hausmann et al., 2019). Elemental ratios analyses in limpets (*Patella* sp.) are particularly interesting because these are the most frequent in shell middens across the European Atlantic façade. The large number of them, and the fact that they are extracted from stratigraphic units in archaeological contexts with precise excavation techniques and absolute and relative dating, make it possible robust statistical studies and to extract valuable paleoclimatic information.

Elemental ratios have been measured with a variety of spectrometric techniques such as Inductively Coupled Plasma-Optical Emission Spectroscopy (ICP-OES), Inductively Coupled Plasma-Mass Spectroscopy (ICP-MS) and Laser Ablation Inductively Coupled Plasma-Mass Spectroscopy (LA-ICP-MS) have been used (Bougeois et al., 2015; Schöne et al., 2011; Martínez-Minchero et al., 2023), but Laser-Induced Breakdown Spectroscopy (LIBS) is emerging as a promising tool with advantages such as multi-elemental analysis, minimal sample preparation, rapid measurements and low cost for both the instrumentation and operation, as no reagents or consumable materials are needed (García-Escárzaga et al., 2015, 2018, 2021; Hausmann et al., 2017, 2023). Laser-based techniques have the advantage of high spatial resolution of the order of microns (the laser spot size), and measurements are usually performed along a single line path across one of the shell's layers, for example, the m+2 calcite layer for *Patella vulgata* (MacClintock, 1967). This contrasts with other methods (isotope ratios, ICP-MS …) in which complete growth increments are drilled or milled and sampled, destroying the shell section from the edge to the apex. Although this process is time-consuming and implies the treatment of the sample, it has the advantage that a large volume of material within the same growth increment is analysed, which should provide less noisy Mg/Ca data in comparison to involving a single sampling point for each growth increment.

In this context, our study introduces a novel approach named "virtual sampling" (VS). This technique tries to imitate, using data processing, the procedure performed for isotopic analysis, that is, the sampling of shell material by milling along the growth lines. Unlike the traditional LIBS processing approach that relies on a single linear scanning line, VS utilises two-dimensional spatial information of the shell (Hausmann et al., 2019, 2023) to derive the temporal sequence of ratios. By incorporating the information provided in the dimension of the isochronous growth lines, VS aims to provide a more accurate and representative average of the Mg/Ca profile. This innovation is expected to produce less noisy data, enabling an enhancement in the precision of the estimation of the seawater temperature variability and, therefore, a better interpretation of the season of collection. Here, twenty-four modern specimens of the limpet *P. vulgata* Linnaeus, 1758 of known collection date, and six archaeological samples, will be analysed to discuss the performance of the VS technique.

2. Materials and methods

2.1. LIBS for the elemental analysis of mollusc shells

LIBS operates by laser ablation of the sample, leading to light emission and plasma formation as a result of atom ionization, in this case within the shell carbonate. The radiation emitted by the sample is collected by some input optics and transferred by an optical fiber to a spectrometer. This radiation is formed by emission lines at different wavelengths corresponding to each chemical element in the sample. Other spectrometric techniques simply use a range of calibration standards to estimate the molar concentration of the elements that contribute to the sample. However, deriving this information from LIBS data is considerably more challenging. This is due to the matrix effect and the absence of calibration standards, for example, of biogenerated carbonates (Winefordner et al., 2004). A simple method to analyse the retrieved spectral information of the sample is based on choosing some suitable emission lines, in this case associated with Mg and Ca, and calculate the ratio of their corresponding intensities (García-Escárzaga et al., 2015; Hausmann et al., 2017; García-Escárzaga et al., 2018; Hausmann et al., 2019; Hausmann et al., 2023). The intensity of the spectral lines can be obtained by the following expression:

$$I^{ki} = F\, C_s\, A_{ki}\, \frac{g_K\, e^{-(E_K/k_B T)}}{U_s(T)}, \quad (1)$$

where I^{ki} is the measured integral line intensity associated with a transition between levels E_k and E_i, F is an experimental factor, C_s is the concentration of the corresponding atomic species s, A_{ki} is the transition probability, g_K is the k level degeneracy, k_B is the Boltzmann constant, T is the plasma temperature and U_s (T) the partition function. It can be observed that the intensity is directly proportional to the concentration. In terms of analysing the seasonality and being able to estimate the season of collection, the Mg/Ca ratio profiles may offer enough information. However, some authors have attempted to provide expressions relating the SST and the Mg/Ca ratios, although the authors indicate that further analysis would be required to obtain a more accurate expression (Garcia-Escárzaga et al., 2021):

$$T_{Mg/Ca} = 0.5492 \cdot \frac{Mg}{Ca} \textit{ratio value} - 8.5532 \quad (2)$$

While the use of line ratios is a valid approach for elemental analysis, it is susceptible to fluctuations caused by variations in the experimental setup, such as optical alignment, temperature changes, or spectrometer configuration. In contrast, the estimation of molar concentration ratios derived from the use of a calibration-free algorithm (CF-LIBS) provides a more robust solution. Martínez-Minchero et al. (2023) used an implementation of the CF-LIBS algorithm to obtain an estimation of the Mg/Ca molar concentration profiles within *Patella depressa* Pennant, 1777 shells. CF-LIBS (Ciucci et al., 1999) is a method enabling the calculation of the elemental concentration of material avoiding the matrix effect, which basically consists of the spectral line intensities of a given element being strongly dependent on the physical and chemical properties of the sample. CF-LIBS also avoids the necessity of employing calibration curves or reference samples and it is not affected by changes in experimental parameters.

To understand how CF-LIBS enables the calculation of the concentration of the different species participating in the plasma, we can first apply logarithm to Eq. (1), so that:

$$\ln\frac{I^{ki}}{g_K A_{ki}} = \frac{-E_k}{k_B T} + \ln\frac{C_s F}{U_s(T)} \tag{3}$$

This equation can be expressed as a linear equation like:

$$y = mx + q_s, \tag{4}$$

where x is E_k. Each emission line considered in the analysis can be represented as a point in the 2D Boltzmann plane defined by the x and y coordinates of Eq. (3). Every atomic species can be represented by a line whose slope m is related to the plasma temperature T and the intercept q_s (the third term of Eq. (3)) is related logarithmically to the species concentration Cs. The concentration of the species can then be calculated as follows:

$$C_s = \frac{1}{F} U_s(T) e^{q_s} \tag{5}$$

A Saha–Boltzmann plot (combination of Boltzmann excitation distribution and Saha ionization distribution) must be used in CF-LIBS to obtain a more accurate value of T (Martínez-Minchero et al., 2023). The use of CF-LIBS is limited by some assumptions about the plasma conditions: the ablation process should be stoichiometric, which means that the composition of the plasma is a representation of the actual composition of the sample before the ablation; the plasma is in local thermodynamic equilibrium (LTE) (Griem, 1963); and that the spectral lines are optically thin (Marotta, 1994). As explained in a previous work, we can assume that these assumptions are met with our experimental setup (Martínez-Minchero et al., 2023). In particular, the Ca and Mg emission lines selected in our study are presented in Table 1.

We have developed a MATLAB implementation (code available at https://github.com/acobo/CFLIBS; please note that MATLAB is required to run the code) of the CF-LIBS based on the following procedure. First, the acquired spectra are normalized and equalized using a previously recorded (by means of an irradiance calibrated lamp) response of the spectrometer. The algorithm uses emission lines previously defined in the code (see Table 1). These lines have been selected based on quality criteria: overlapped, highly auto-absorbed, low intensity or saturated lines are discarded. The background radiation (baseline) is removed via the airPLS algorithm (Zhang et al., 2010) and the fitting of the emission lines is evaluated: for each emission line its spectral range is determined, and it will be used for each spatial position on the sample. After that, the average spectrum for each spatial position is calculated and the peak fitting of the emission lines is performed, allowing the estimation of the fitting error and the labelling of lines not suitable for the Boltzmann-plots, which are used to obtain the plasma temperature. The plasma electronic density is calculated for all the emission lines with a known value for the Stark constant w and also for the H-alpha line. Finally, using those temperature and electronic density estimations, an iterative calculation of the Saha-Boltzmann plot allows to obtain the concentrations of the species under analysis.

The experimental setup employed to perform the LIBS analysis is presented in Fig. 1. The LIBS setup is formed by a neodymium-doped yttrium aluminium garnet (Nd:YAG) Q-Switched double-pulsed laser (Lotis LS-2134D) operating at 10 Hz and with an output wavelength of 1064 nm. A lens with a focal length of 75 mm is used to focus the laser beam, resulting in the sample material ablation forming a spot on the sample of 100 μm diameter. The plasma radiation generated by the pulses, maintained at 35 mJ, is collected by an optical fibre (1 mm diameter) attached to a fibre-coupled 8-channel Avantes ULS2048-USB2-RM spectrometer with an input slit of 5 μm, a spectral range from 178 to 889 m and a resolution from 0.015 to 0.06 nm (channel dependent). The sample surface can be inspected via a trough-lens vision system with a CCD camera and the specimen positioning is managed by a motorized XYZ positioner, programmed to perform a 2D scan within a previously specified area within the shell surface under analysis.

Table 1
Spectroscopic information of the Ca and Mg atomic lines employed in the CF-LIBS calculations. Data from the NIST Atomic Spectra Database (Kramida et al., 2023).

Element	Ionization	Wavelength (nm)	A_{ki} (s^{-1}) x 10^8	g_k	E_k (eV)	k_t
Ca	I	227.55	0.30	3	5.45	11.11
Ca	I	239.86	0.17	3	5.17	7.61
Ca	I	558.20	0.06	7	4.74	5.63
Ca	II	315.89	3.10	4	7.05	7.45
Ca	II	370.60	0.88	2	6.47	1.98
Ca	II	373.69	1.70	2	6.47	3.86
Mg	I	382.94	0.90	3	5.95	14.84
Mg	I	516.73	0.11	3	5.11	5.99
Mg	I	517.27	0.34	3	5.11	17.96
Mg	I	518.36	0.56	3	5.11	24.04
Mg	II	279.55	2.60	4	4.43	415.30
Mg	II	280.27	2.57	2	4.42	208.03

2.2. Mollusc shells selected

To validate the proposed technique, twenty-four *P. vulgata* modern specimens collected on different dates between 2011 and 2012 in Langre Beach [Ribamontán al Mar, Cantabria (northern Spain)] have been studied. Fig. 2 shows the geographical location of Langre Beach and the specific location of collection in different distance scales, while Fig. 3 shows specimens of *P. vulgata* and *P. depressa* at Langre Beach. Basic information about these specimens is provided in Table 2 (additionally, images of the scanned surfaces of each specimen can be observed in the complementary material associated with this submission).

In addition to the analysis of the modern specimens, a study of six archaeological *P. vulgata* specimens has also been conducted in order to test this method on archaeological samples from the same species and close geographical location. The assemblage was selected from the Mesolithic shell midden of El Toral III cave, located in the municipality of Llanes (Asturias, Spain), approximately 1 km away from the modern coastline (Noval-Fonseca, 2013) (Fig. 4). The shell midden occupation levels reflect a chronological range of 9891–9494 cal BP to 7388–6656 cal BP, according to previous studies (Arniz-Mateos et al., 2024). Each of the selected archaeological specimens came from a different stratigraphic excavation unit and chronological adscription detailed in Arniz-Mateos et al. (2024). The samples were identified indicating the abbreviation of the archaeological site of El Toral III cave ("TOR"), the number of the stratigraphic unit, the individual number of the specimen and the initials according to the species to which it belongs, in this case *P. vulgata* (PV). All the specimens were measured and weighed as indicated in Table 3, where the specimens are listed from top to bottom in chronological order of their stratigraphic units.

2.3. Biological and ecological aspects of *Patella vulgata* Linnaeus, 1758

The common European limpet, *P. vulgata*, is an intertidal gastropod inhabiting rocky shorelines from Norway to northern Spain, particularly around the British Isles (Blackmore, 1969), with lifespan greatly affected

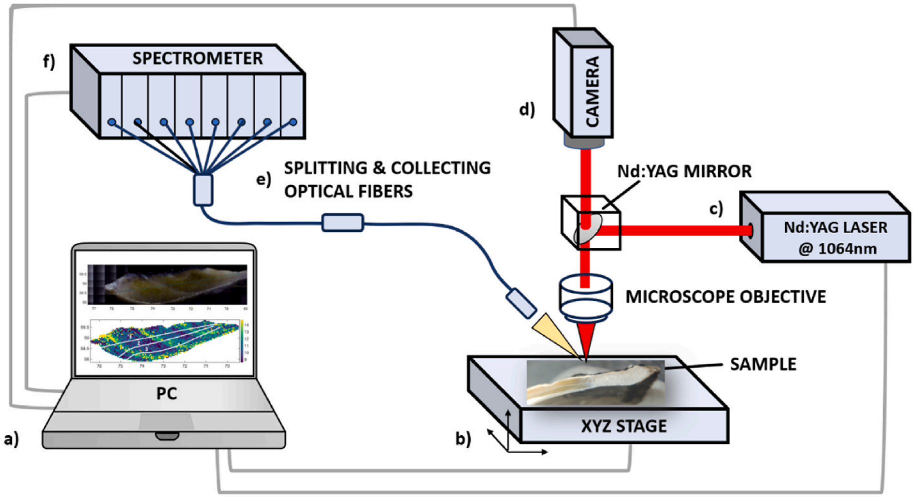

Fig. 1. Experimental setup used to perform the LIBS analysis of the limpet shells: a) PC for device control and processing; b) motorized xyz stage to move the sample and perform the LIBS scans; c) Nd:YAG laser use to ablate the sample surface and generate the associated plasma radiation; d) camera used to record the sample surface and determine the scanning area; e) optical fibre guiding the plasma optical radiation to the spectrometer; f) 8-channel spectrometer.

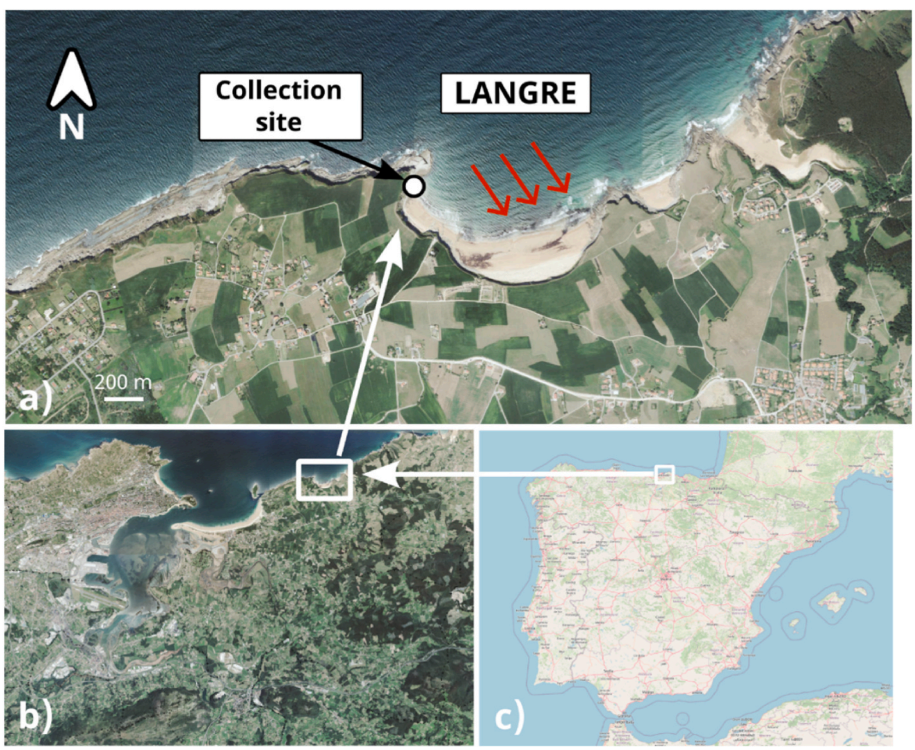

Fig. 2. Image showing the location of the collection site: (a) detail of Langre Beach at Ribamontán al Mar (Cantabria), arrows indicate the direction of waves; (b) location of Langre Beach on the coast of the Cantabrian Sea, near the city of Santander (on the top-left part of the image); (c) detail of the location on the map of the Iberian Peninsula. (a) and (b) created using data from the Government of Cantabria, available for free at https://mapas.cantabria.es; (c) the image was created using data from OpenStreetMap, which is freely available under the Open Database License (ODbL).

by their corresponding habitats, ranging from 2 to 3 to 15–17 years (Little et al., 2017). *P. vulgata* tolerates temperatures from −8.7 to 42.8 °C and salinities from 20 to 35 psμ, although extreme temperatures slow shell growth (Crisp, 1965; Branch, 1981). The shell, conical and cap-shaped, averages 2–4 cm, with a grey to white exterior and a smooth interior marked by a muscle scar (Fig. 5). Growth rates, ranging from 0.005 to 2.6 mm/month, are primarily temperature-dependent, with winter growth lines in higher latitudes and summer growth slowdowns in lower latitudes; with reproduction and food supply also affecting their growth (Blackmore, 1969; Ekaratne and Crisp, 1984).

2.4. Environmental setting

To provide a better understanding of the performance of the proposed technique, the evolution of the SST at El Bocal site, in the Bay of Santander and close to Langre Beach, is shown in Fig. 6. The SST directly provided by the sensor is shown by the grey line, while a smoothed evolution of the SST has been represented (black line) by using a Savitsky-Golay filter.

Fig. 3. Specimens of *Patella* sp. at Langre Beach, Cantabria (Spain). Photographs taken by Rosa Arniz-Mateos.

Table 2
Biometrical data of the *P. vulgata* shells collected in Langre between November 2011 and August 2012 selected for this study.

Sample	Length (mm)	Width (mm)	Height (mm)	Weight (g)	Date of collection
LAN96	21.32	24.2	11.2	2.0	November 12, 2011
LAN98	24.55	20.12	10.86	1.4	November 12, 2011
LAN100	30.57	25.88	14.26	3.4	November 12, 2011
LAN105	27.47	22.44	10.48	1.5	November 12, 2011
LAN109	32.58	27.48	14.37	2.8	November 12, 2011
LAN122	30.5	24.33	9.98	2.1	November 12, 2011
LAN176	27.8	22.9	11.3	1.7	February 23, 2012
LAN177	34.5	28.5	13.3	3.7	February 23, 2012
LAN178	28.6	23.2	11.1	2	February 23, 2012
LAN182	33.8	27.4	11.2	2.9	February 23, 2012
LAN183	27.9	22.9	13.2	2	February 23, 2012
LAN184	31.8	26.9	10.6	2	February 23, 2012
LAN229	32	25.3	13.8	2.5	June 3, 2012
LAN230	31.8	24.4	13.9	2.5	June 3, 2012
LAN231	34.1	29.1	15.5	3.7	June 3, 2012
LAN235	31.1	25.3	14.1	2.3	June 3, 2012
LAN236	32.5	26.5	13.9	2.7	June 3, 2012
LAN237	31.6	25.4	11.4	1.9	June 3, 2012
LAN254	31.1	26.8	13.6	2.8	August 5, 2012
LAN255	32.4	26	13.3	3.3	August 5, 2012
LAN256	28.5	23.5	13.2	1.9	August 5, 2012
LAN258	33.5	27.6	13.3	2.8	August 5, 2012
LAN259	34.4	27.2	12.4	2.4	August 5, 2012
LAN261	29.9	24.6	12.3	2.2	August 5, 2012

2.5. Sampling procedure

For this study, instead of the linear sampling through the centre of the m+2 calcite layer, the shell sections have been measured on a 2D grid (Hausmann et al., 2019, 2023) of spatial points 50 μm apart. In each spatial point the five LIBS spectra are averaged and from the spectral information the molar ratio Mg/Ca is obtained by using an implementation of the calibration-free LIBS algorithm (Ciucci et al., 1999) available at https://github.com/acobo/CFLIBS.

Once these 2D maps have been acquired, there is no longer a need to make a 1D (linear) scanning of the limpet to generate the profile of the Mg/Ca ratio for the estimation of the season of collection, but the 2D maps can be directly used via software to deploy different trajectories on the shell to analyse the associated Mg/Ca profiles. Fig. 7 presents an example of a 1D scanning with specimen LAN183 (*P. vulgata* collected in the Cantabrian region, northern Iberia). Fig. 7(a) shows the shell disposed in the setup, with the apex (not entirely visible) to the left and the last biomineralised material on the bottom-right edge. Fig. 7(b) shows the Mg/Ca ratio profile associated with the linear path highlighted in Fig. 7(a). Given the known relationship between the Mg/Ca ratio and the seawater temperature, well-defined seasonal cycles associated with the cyclic temperature variations through the lifespan of the limpet would be expected in the Mg/Ca ratio evolution (Schöne et al., 2008; García-Escárzaga et al., 2018, 2021; Hausmann et al., 2021). In particular, the Mg/Ca ratio in the late part of the sequence (the one closer to the shell edge, i.e., the date of collection) is especially important to infer the season of collection in archaeological samples by comparison of those final points with the previous ratio values in the sequence. For example, an increasing trend in the late part of the sequence would indicate spring as the collection season, while high ratio values, similar to the maximum values of the previous seasonal cycles in the sequence, would suggest a collection at the end of the summer when water temperatures peak. As can be observed in this example, it may be challenging to estimate the season of collection [specimen LAN183 was collected in winter (February)].

Fig. 8 (a) shows the Mg/Ca 2D map associated with LAN183, where lighter (green, yellow) colours indicate higher Mg concentrations. Again, the shell edge at the bottom right corresponds to the collection date. A simple visual inspection of the 2D map may help in the estimation of the season of collection, as three different sections with growth lines showing higher Mg/Ca concentrations can be easily identified. A winter collection season for this specimen would be consistent with this interpretation: darker colours, lower Mg/Ca ratios, and near the shell edge. However, a more quantitative approach would be desirable, especially if it enables a comparison with the traditional linear profiles. The acquisition of the Mg/Ca 2D maps allows us to plot different linear trajectories and the retrieval of the corresponding Mg/Ca profiles, enabling a better understanding of these profiles and the identification of possible artefacts. For example, Fig. 8(b) shows the Mg/Ca profile associated with the trajectory "1" deployed on the 2D map of Fig. 8(a). Even if the trajectory is almost the same as the one described in Fig. 8(a), the retrieved profile is similar but with some differences: for example, an artefact with a higher Mg concentration appears at $x \approx 2.7$ mm. The Mg/Ca profile presented in Fig. 8(c) is less noisy (it can be appreciated by the depicted error bars (in grey), calculated as the standard deviation of the ratio values in each spatial point from the five laser shots) and the cyclicity can be better appreciated. Fig. 8(d) shows the result of choosing a trajectory going through the bottom part of the m+2 calcite layer.

This example represents the relevance of choosing an appropriate linear trajectory for a correct estimation of the season of collection and even gives rise to the question of whether these linear trajectories are suitable for the estimation of the season of collection. In fact, it can be easily observed that the region closer to the shell edge (critical in terms of a correct estimation of the season of collection) does not have a uniform Mg/Ca ratio, even if it is supposed to be isochronous. However, the data available in the 2D map enables an improvement in this procedure by identifying the direction of the growth lines and using the Mg/Ca ratios through these lines to perform an average in that dimension, which should improve the results and, consequently, the interpretation of the Mg/Ca profiles and the associated season of collection for each specimen. The proposed algorithm is derived from the experience of the co-authors in past sclerochronological studies of this species (Surge et al., 2013), in particular the following assumptions: 1) the edge of the m+2 calcite layer is isochronous and has the last biomineral created by

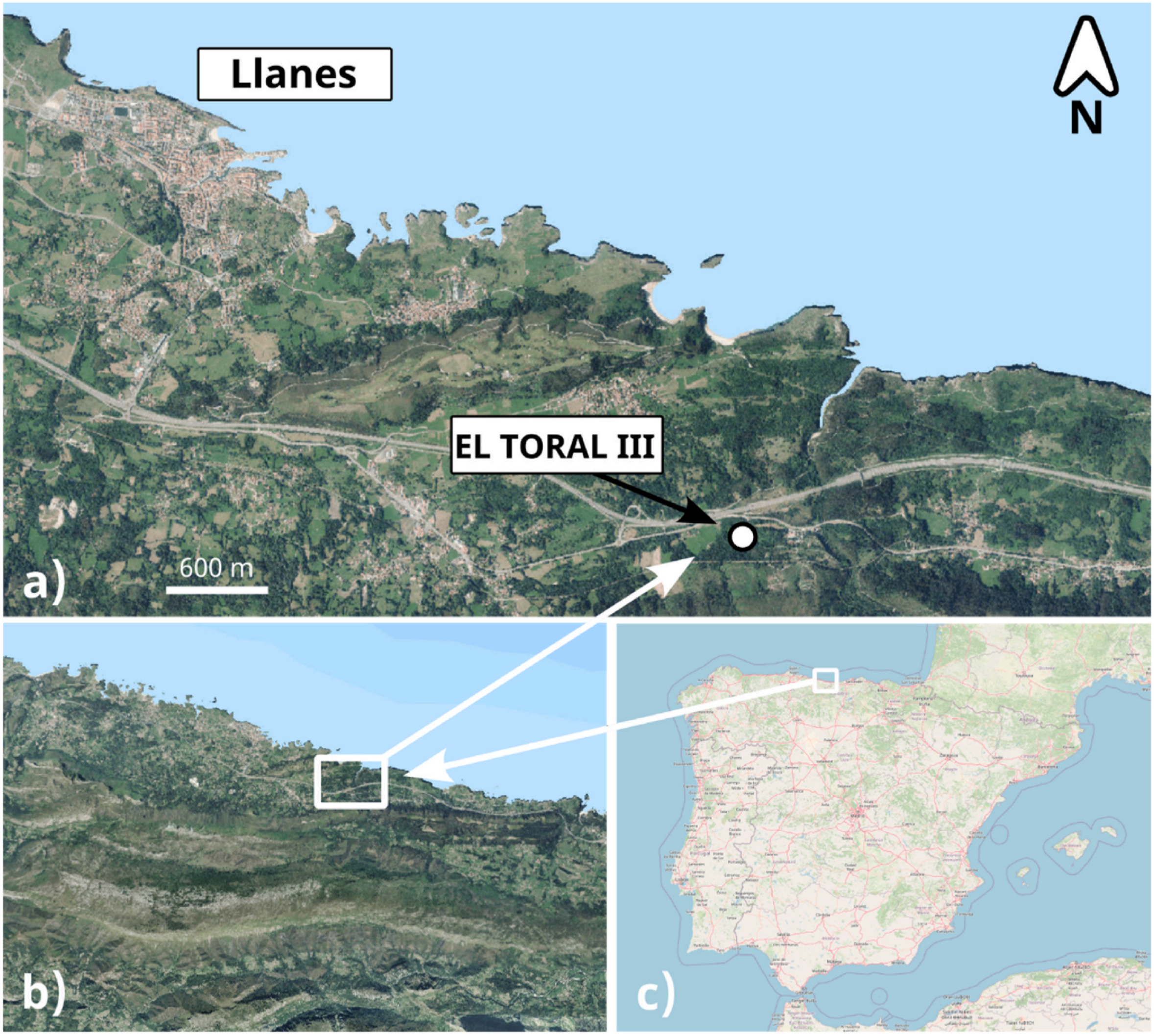

Fig. 4. Geographical location of the collection site of the archaeological specimens: (a) detail of the geographical area of El Toral III cave close to Llanes (Asturias); (b) Detailed location of El Toral III close to the coast of the Cantabrian Sea; (c) detail of the location on the map of the Iberian Peninsula. (a) and (b) created using data from the Government of Asturias, available for free at https://ideas.asturias.es/; (c) the image was created using data from OpenStreetMap, which is freely available under the Open Database License (ODbL).

Table 3
Biometrical data of the *P. vulgata* archaeological specimens from the shell midden site of El Toral III (Arniz-Mateos, 2024).

Specimen	Length (mm)	Width (mm)	Height (mm)	Weight (g)
TOR.13C.9.PV	28.5	22.2	10.2	1.6
TOR.22.3.PV	27.6	22.2	10.2	1.7
TOR.19.3.PV	28.4	22.3	10.8	2.1
TOR.21.3.PV	30.5	22.5	11.7	2.2
TOR.20.5.PV	25.9	21.7	11.6	1.9
TOR.17.3.PV	27.8	22.7	9.9	1.6

the mollusc (Fenger et al., 2007), 2) adjacent growth lines have almost the same shape, so the shape of the edge can be used as a starting point, and 3) the Mg/Ca ratio at any given spatial point is dependent on the water temperature and an unknown biological or environmental mechanism that randomly adds or subtracts to the temperature-dependent value. The last assumption is supported by the fact that none of the published 2D Mg/Ca maps (Hausmann et al., 2023) show spatial patterns other than the growth lines. The algorithm has been implemented as follows (code available at https://github.com/acobo/virtualSampling):

1. On the 2D map, a linear trajectory is manually defined through the middle section of the m+2 calcite layer.
2. A line is drawn following the shell edge and stored as the initial reference shape of a growth line (this step will be automated in future versions of the algorithm).
3. The linear trajectory is scanned with pre-defined distance steps (e.g., 50 μm), and, for each point, a new shape of the isochronous growth line is calculated by means of an optimisation algorithm that tries to find a polyline that minimises the relative standard deviation (RSD) of the ratios along that line. Control points of the polyline are restricted to being modified to a certain amount from the previous point.
4. The Mg/Ca ratio in each spatial point of the linear trajectory is calculated as the average along each growth line.
5. All the averaged ratio values give rise to a new 1D Mg/Ca profile.

3. Results

The working principle and an example of the application of the VS technique are presented in Fig. 9, where the 2D Mg/Ca map associated with specimen LAN183 (collected in February (winter season)) is shown in Fig. 9(a), as well as the Mg/Ca profiles obtained by using a single

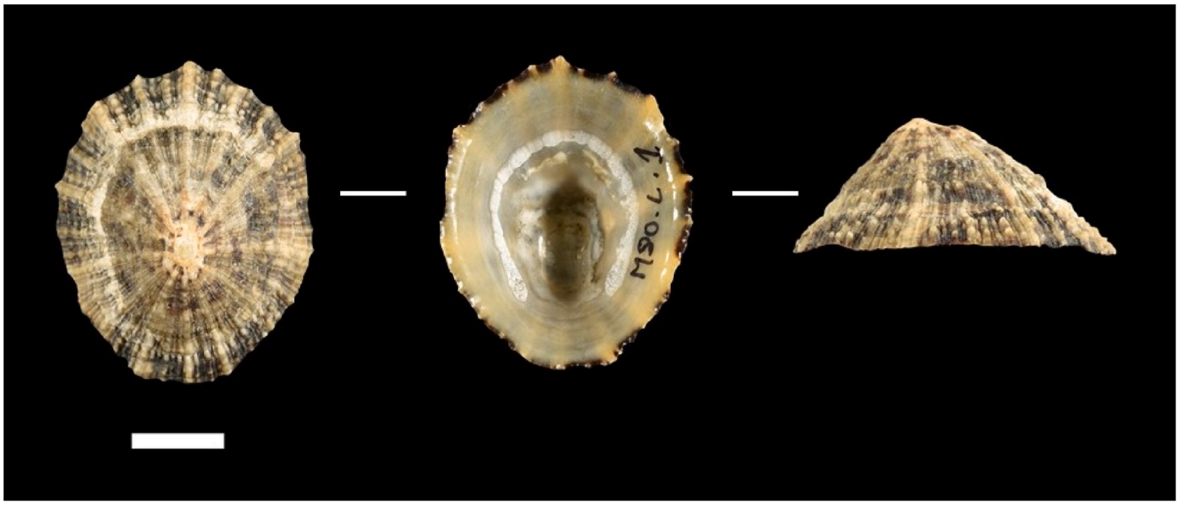

Fig. 5. Modern specimen of *P. vulgata.* Top view, interior view, and side view (from left to right). Scale 1 cm.

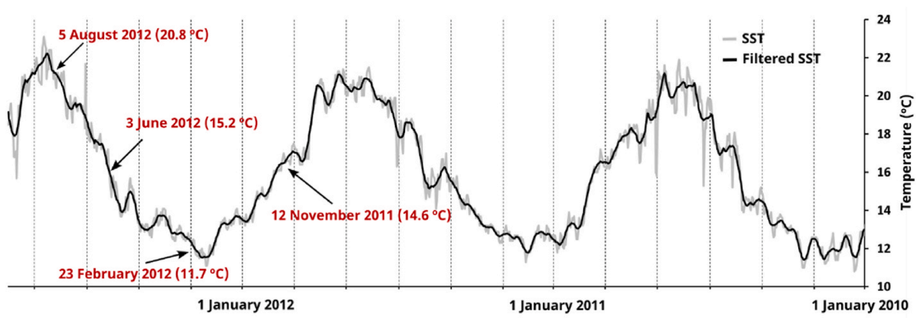

Fig. 6. Evolution of the SST at Langre Beach between January 1, 2010 and October 1, 2012 [Data courtesy of the Centro Oceanográfico de Santander (COST), Instituto Español de Oceanografía (IEO, CSIC)].

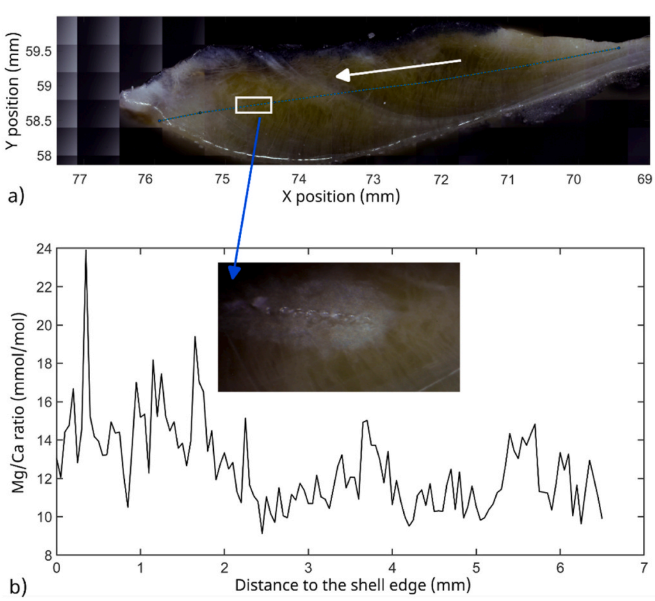

Fig. 7. (a) Shell surface for LIBS analysis of specimen LAN183 (the white arrow indicates the scanning direction); (b) Mg/Ca profile for specimen LAN183; (inlay) detail of the craters generated by the laser shots on the m+2 calcite layer.

linear scan (Fig. 9(b)) and by means of the VS technique [Fig. 9(c)]. The same data, in this case associated with LAN178, also collected in February, is presented in Fig. 10.

Two different specimens collected in August (Summer season) are presented in Fig. 11 (LAN256) and 12 (LAN259). Additionally, other specimens have also been analysed and their corresponding results can be observed in the Supplementary Materials. Figures S2 (LAN235) and S.3 (LAN237) present the results associated with the analysis of two limpets collected in June (spring season).

Figures S4 and S5 show the results of the analysis performed on LAN100 and LAN105, collected in November (autumn season). Figure S6 also presents the results derived from the analysis of LAN229, collected in spring, where it can be observed that it is difficult to clearly identify the evolution of seasonal cycles.

As an extension of the proposed solution, Fig. 13 presents the same analysis of the Mg/Ca profile via the VS technique but also shows by means of a grey band the maximum and minimum values of the Mg/Ca ratio along all the growth lines considered during the process. Results for specimen LAN183 (Fig. 13(a)) and LAN178 (Fig. 13(b)) are shown.

Six archaeological specimens of *P. vulgata* from different stratigraphic units selected of El Toral III site have also been analysed and the results are presented in Fig. 14 (TOR.13C.9. PV) and Fig. 15 (TOR.19.3. PV). The results associated with specimens TOR.22.3. PV (Fig. S7), TOR.21.3. PV (Fig. S8), TOR.20.5. PV (Fig. S9) and TOR.17.3. PV (Fig. S10) are presented in the Supplementary Materials.

Fig. 16 presents the same analysis already performed in Fig. 13 for contemporary specimens, in this case with archaeological specimens TOR.17.3. PV (Fig. 16(a)) and TOR.22.3. PV (Fig. 16(b)). The grey bands

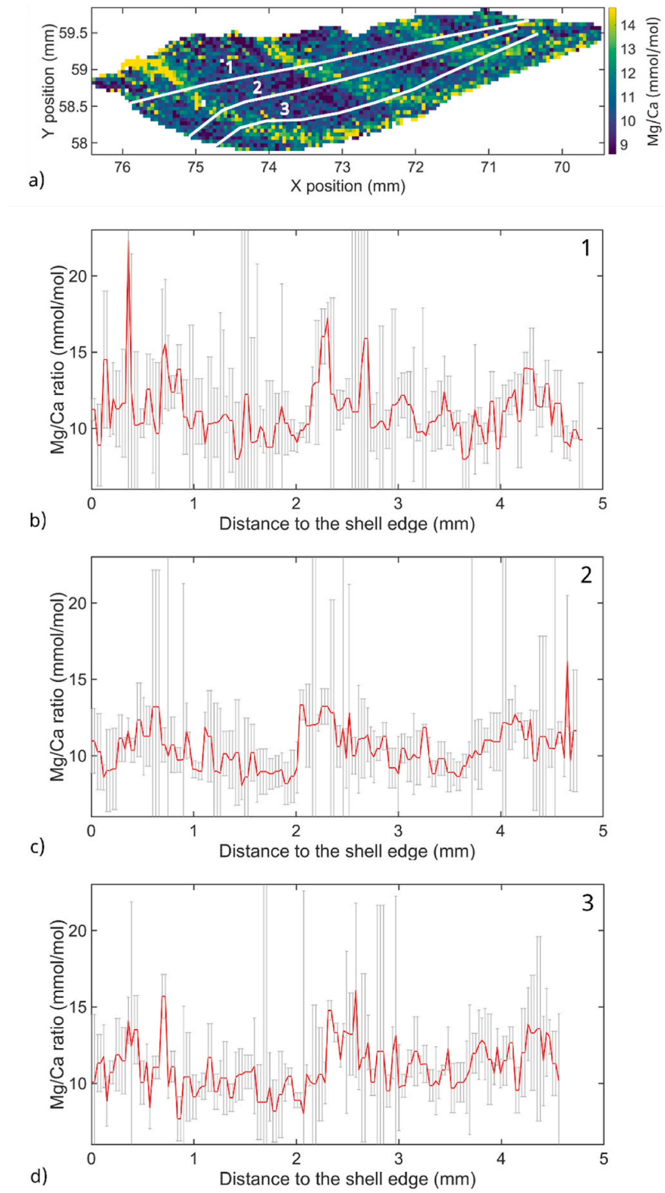

Fig. 8. (a) Mg/Ca 2D LIBS map for specimen LAN183 (collected in February, winter season); (b) Mg/Ca profile for trajectory 1; (c) Mg/Ca profile for trajectory 2; (d) Mg/Ca profile for trajectory 3. Error bars (in grey colour) have been calculated as the standard deviation of the ratio values in each spatial point from the five laser shots. (For interpretation of the references to colour in this figure legend, the reader is referred to the Web version of this article.)

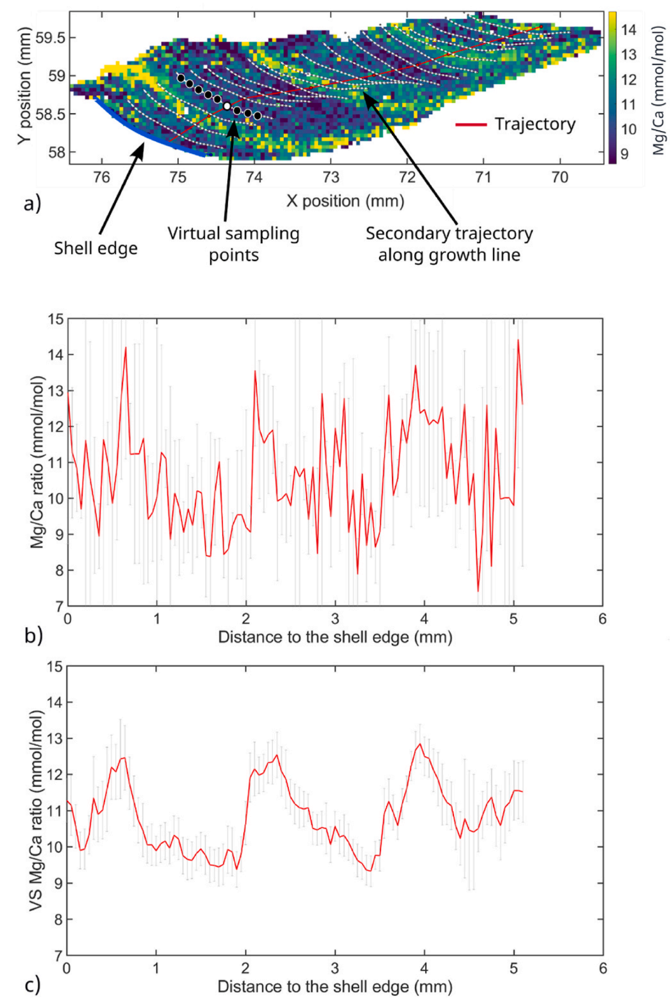

Fig. 9. (a) Illustration of the working principle of the virtual sampling technique with the Mg/Ca 2D map of specimen LAN183 (collected in February, winter season); (b) Mg/Ca profile of LAN183 using a single linear trajectory; (c) Mg/Ca profile of LAN183 using virtual sampling.

show the maximum and minimum values of the Mg/Ca ratio along all the growth lines considered during the process.

4. Discussion

The differences in the resulting Mg/Ca profiles between the conventional approach using a single linear path and the employment of virtual sampling utilising the associated 2D map are remarkable. The application of virtual sampling to specimen LAN183 (collected in February, Winter season) (Fig. 9(c)) gives rise to a smoother profile in comparison to the results obtained in Fig. 9(b). While the profile associated with the latter is somewhat noisier and makes it difficult to distinguish seasonal cycles, the profile presented in Fig. 9(c) is notably clearer, allowing the identification of three clear summer cycles ($x \approx 4$, 2.3 and 0.7 mm), the last close to the shell edge beginning a decrease in the Mg/Ca ratio followed by an increase close to $x \approx 0$ mm. Even if the use of the VS technique clearly improves the Mg/Ca profile, the final increase trend seems to contradict a season in the winter collection. We have found that, albeit the proposed solution gives more accurate ratio profiles, the interpretation of the season of collection in some specimens remains problematic. The error bars have been plotted to enable a qualitative analysis of the effect of the VS technique even if some of them exceed the limits of the vertical axis in Fig. 9(b), as the same vertical range has been preserved in the representation of Fig. 9(b) and (c) to allow a better comparison.

Results associated with the shell of another limpet collected in Winter, specimen LAN178, are presented in Fig. 10. In this case a summer season around $x \approx 5$ mm can be easily identified, as well as near the end of the life of the specimen ($x \approx 0.5$ mm), and therefore, a season of collection in winter might be consistent with the interpretation of the graph, given that there is a clear decreasing Mg/Ca ratio trend between $x \approx 0.5$ mm and $x = 0$ mm.

Fig. S2(a) presents the Mg/Ca 2D map associated with specimen LAN235 (collected in June, spring season). In this case the number of cycles associated with different seasons is reduced, with a peak in the Mg/Ca ratio (summer) that can be located in the VS profile (Fig. S2(c) around $x \approx 1$ mm, but whose location would be more complicated if only Fig. S2(b) was available. The profile seems consistent with a collection in spring, as an increasing trend appears in the vicinity of the shell edge

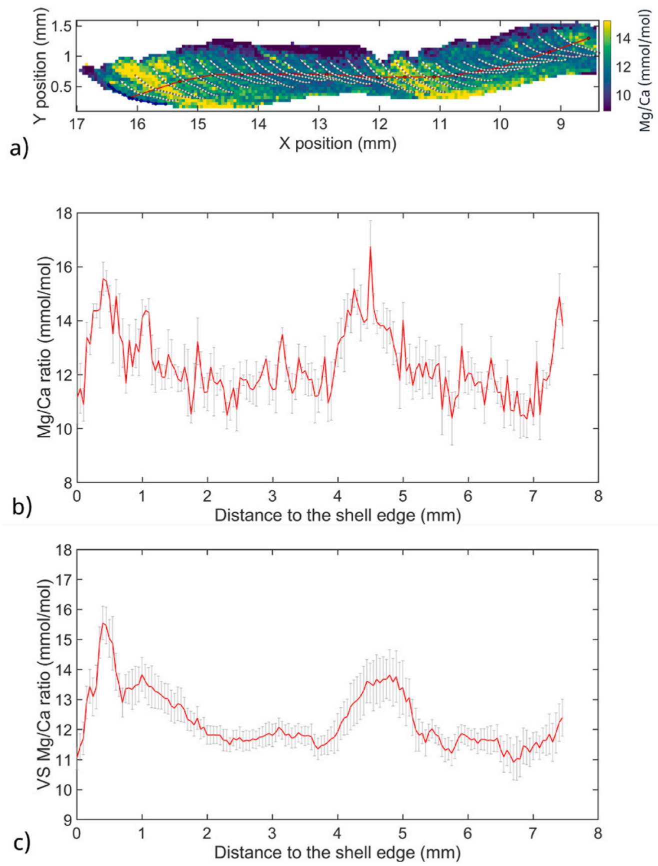

Fig. 10. (a) Mg/Ca 2D map of specimen LAN178 (collected in February, winter season); (b) Mg/Ca profile of LAN178 using a single linear trajectory; (c) Mg/Ca profile of LAN178 using virtual sampling.

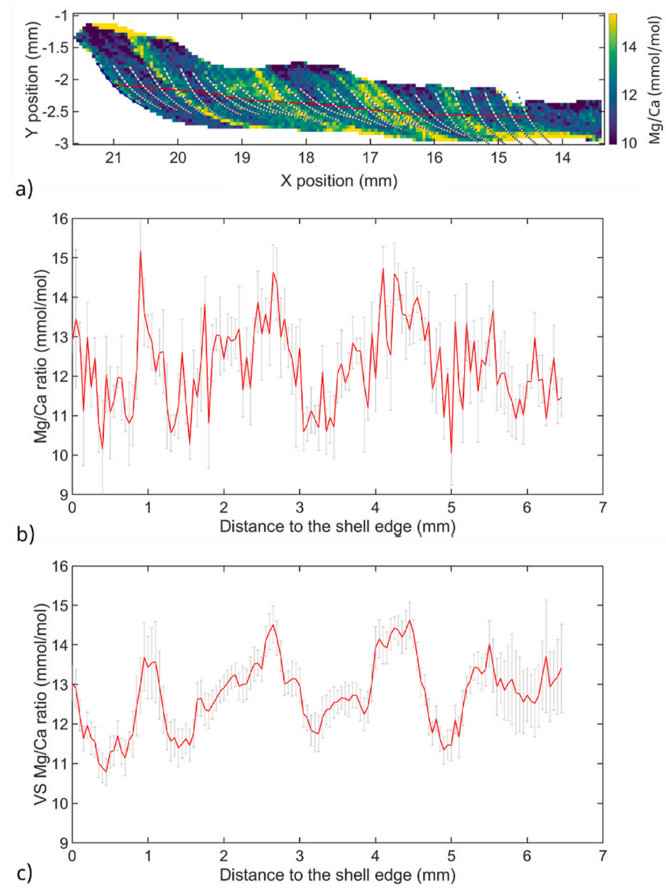

Fig. 11. (a) Mg/Ca 2D map of specimen LAN256 (collected in August, summer season); (b) Mg/Ca profile of LAN256 using a single linear trajectory; (c) Mg/Ca profile of LAN256 using virtual sampling.

after the winter period. Specimen LAN237, also collected in spring and analysed in Fig. S3, shows an interesting Mg/Ca profile, as an abrupt change can be easily identified at x ≈ 4 mm (Figures S3(b) and (c)), corresponding to the location where the section with a high Mg/Ca ratio at the middle of the shell ends [x ≈ 18 mm in the 2D map of Fig. S3(a)]. The cycle associated with a summer season is more evident in Fig. S3(c) via the VS method, and the end of the profile towards x = 0 mm is more compatible with a collection in spring in Fig. S3(c) than in Fig. S3(b).

Figs. 11 and 12 present the results for two specimens collected in August (summer season). Specimen LAN256 is analysed in Fig. 11 and, again, the comparison of Fig. 11(b) and (c) shows the relevant improvement achieved with the VS technique. In this case, in particular, the variance in the profile of Fig. 11(b) makes it complicated to detect some of the season cycles that can be easily observed in Fig. 11(c) and suggests summer as the season of collection. It is also interesting to note that the last complete summer period (x ≈ 1 mm) is shorter than the three previous summers. This could be explained by the tendency of older specimens to exhibit more frequent growth stoppages and, in general, a less stable growth pattern (MacClintock, 1967). Results for specimen LAN259, also collected in August, are presented in Fig. 12. In this case the profile seems to be consistent with a collection in summer although an abrupt pattern appears after the summer period (x ≈ 3.5 mm in Fig. 12(c)). This abrupt change, very similar to the one already discussed in Fig. S3(c) could be associated with a growth stoppage, which are frequently found in *Patella* sp. and thought to be a response to high or low temperatures outside their thermal tolerance levels (García-Escárzaga et al., 2020).

To end the analysis of limpets collected in all the seasons, Figures S4 and S5 show the analysis of two specimens collected in November (autumn season): LAN100 and LAN105.

The 2D Mg/Ca map of LAN100 shown in Fig. S4 (a)and the resulting Mg/Ca profiles indicate a limpet that has lived through four summer seasons, five if the first one at x ≈ 7.3 mm in Fig. S4 (b) and (c) is considered. It is worth noting how the use of the VS method remarkably improves the detection of the seasonal cycles in this case. The trend of the Mg/Ca profile near the shell edge could be consistent with a collection in autumn or even winter.

Finally, Fig. S5 presents the analysis performed on specimen LAN105. In this case, both the 2D map (Fig. S5 (a)) and the VS profile (Fig. S5 (c)) indicate two regions with growth lines with higher Mg concentration (x ≈ 7.5 mm and in the region close to the shell edge). Consequently, this specimen seems to have lived through only two different summers, and the Mg/Ca evolution close to the shell edge also indicates a possible collection in autumn, with a relevant difference in the noise associated with the Mg/Ca profiles in this case.

As already commented, the proposed VS technique clearly improves the Mg/Ca profiles, which can help in the estimation of the season of collection, but in some cases (e.g. the results discussed for specimens LAN183 (collected in winter) or LAN237 (collected in spring)) that estimation is still not clear. As an extension of this method to investigate this behaviour further in different samples, Fig. 13 presents the same analysis via the VS technique but also shows by means of a grey band the maximum and minimum values of the Mg/Ca ratio along all the growth lines considered during the process. Results for specimen LAN183 are shown in Fig. 13(a), where it can be observed that the range of values of Mg/Ca close to the border (x ≈ 0 mm) is wide (from y ≈ 9–14 mmol/mol), preventing an unambiguous identification of the season of collection. This seems to indicate that the influence of other environmental or endogenous mechanisms is significant and prevents any

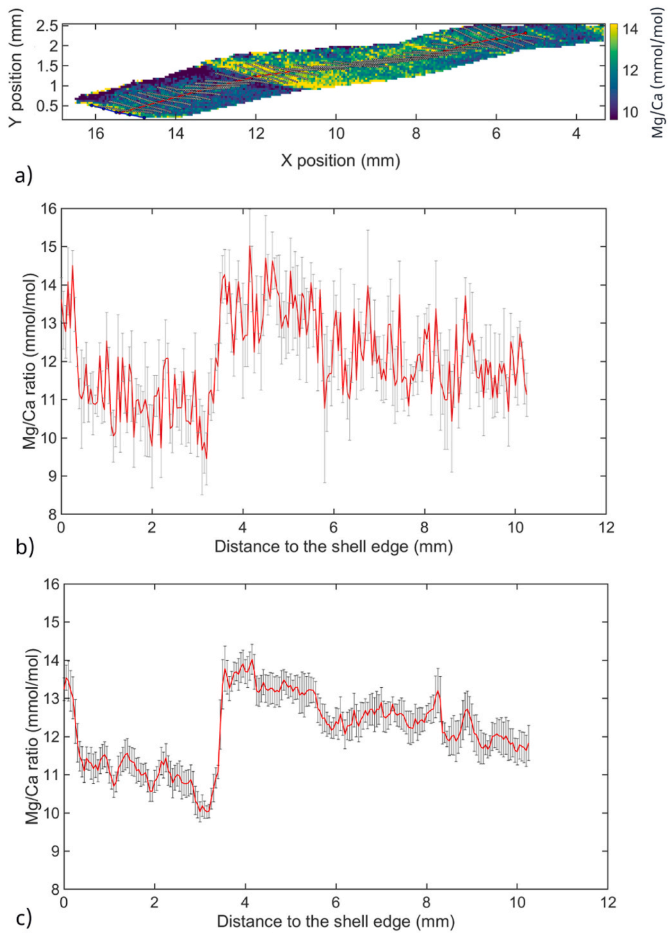

Fig. 12. (a) Mg/Ca 2D map of specimen LAN259 (collected in August, summer season); (b) Mg/Ca profile of LAN259 using a single linear trajectory; (c) Mg/Ca profile of LAN259 using virtual sampling.

paleoclimatic interpretation. However, this is not the case for most of the samples. Fig. 13(b) presents the results associated with LAN178, also collected in winter. In this case, the range of Mg/Ca values at the edge clearly only allows for an estimation (correct in this case) of the winter collection season.

Finally, Table 4 summarizes our estimation of the season of collection for all twenty-four modern samples, derived from the analysis of the standard and VS sequences. It can be shown that most of the specimens show a clear cyclic sequence from which the actual season of collection can be estimated correctly. In particular, 16 out of the 24 specimens analysed via VS have an accurate estimation of the season of collection, implying a 66% success rate. If the limpets collected in temperate seasons (5 incorrect estimates, 4 in spring where it is difficult to observe clear seasonal variations) were excluded, the success rate in the estimation would be over 80%. It is important to note that without the use of the VS method, the overall success rate would drop clearly below 50%, which demonstrates the ability of the proposed solution to improve the results derived from the use of linear LIBS scans. As commented, some specimens show a wrong season or are difficult to interpret, even when enhanced by the VS algorithm. Attending to the results of Table 4, the specimens collected in spring seem to contribute the most to increasing the error rate, with some of them not showing clear seasonal cycles in their Mg/Ca profiles (LAN122 (collected in autumn) and LAN229, LAN230, LAN236 and LAN237 (collected in spring). To illustrate this situation, Fig. S6 shows the results associated with LAN229, where it can be observed that, even if the use of the VS method enhances the Mg/Ca profile, it is difficult to clearly distinguish seasonal cycles, especially

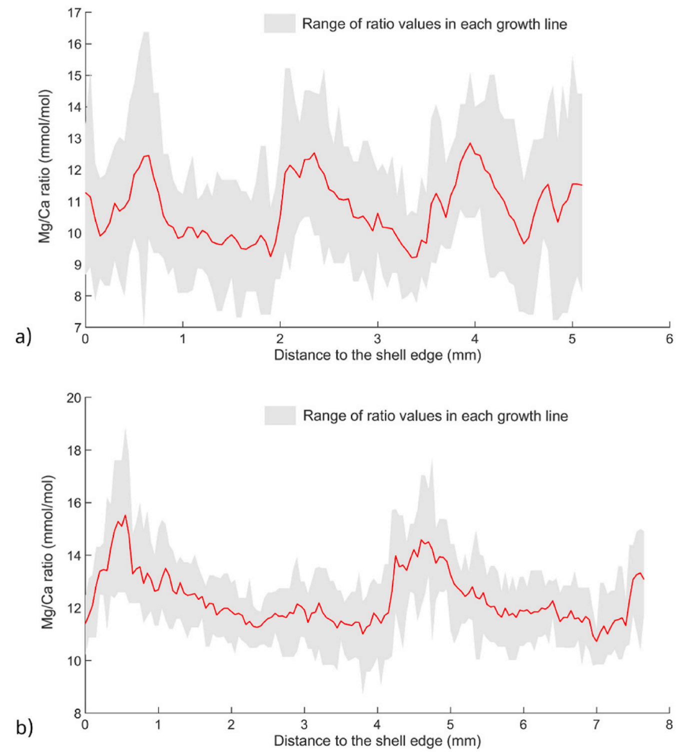

Fig. 13. VS technique and estimation of the maximum and minimum values of the Mg/Ca ratio for each growth line considered in the process: (a) analysis of LAN183; (b) analysis of LAN178.

near the shell edge.

One possible explanation to these ambiguous results for the specimens collected in autumn and mainly in spring might lies in the growth stoppages of these specimens during these periods not allowing a suitable record of their season of collection. However, the growth pauses of *P. vulgata* do not always occur at the same times of the year. For example, a previous study of *P. vulgata* specimens also collected in Langre Beach indicated a greater growth during the spring and a growth pause during the summer and winter (Gutiérrez-Zugasti et al., 2017). Although no sclerochronological studies have been conducted, estimations of the ontogenetic age do not seem to give rise to a possible explanation for this situation. There are also some specific cases (e.g. LAN183) where a clear cyclicity can be observed in the profiles, but the end of the sequence does not correspond to the season of collection (Arniz-Mateos, 2024).

This confirms that, even when the measurement uncertainty is reduced using the VS approach, Mg/Ca ratios are not a reliable proxy in all specimens of *P. vulgata*. This is in line with the mixed results of elemental ratios found in studies of this and other mollusc species (Freitas et al., 2005; Wanamaker et al., 2008b; Schöne et al., 2011; Poulain et al., 2015; Marali et al., 2017). However, this approach will allow future studies to focus on biological and environmental factors influencing the Mg/Ca ratios, improving the reliability of data interpretation and aiding to a better understanding of the potential and limitations of using elemental ratios for archaeological and paleoenvironmental reconstruction.

Apart from the analysis of the 24 modern samples, six archaeological *P. vulgata* specimens from different stratigraphic units of El Toral III cave [Llanes, Asturias (northern Spain)] have also been included in this study. Figs. 14 and 15 present the 2D Mg/Ca maps, Mg/Ca profiles using a single linear trajectory and Mg/Ca profiles using VS for specimens TOR.13C.9. PV and TOR.19.3. PV. The results associated with specimens TOR.22.3. PV (Fig. S7), TOR.21.3. PV (Fig. S8), TOR.20.5. PV (Fig. S9) and TOR.17.3. PV (Fig. S10) are presented in the Supplementary

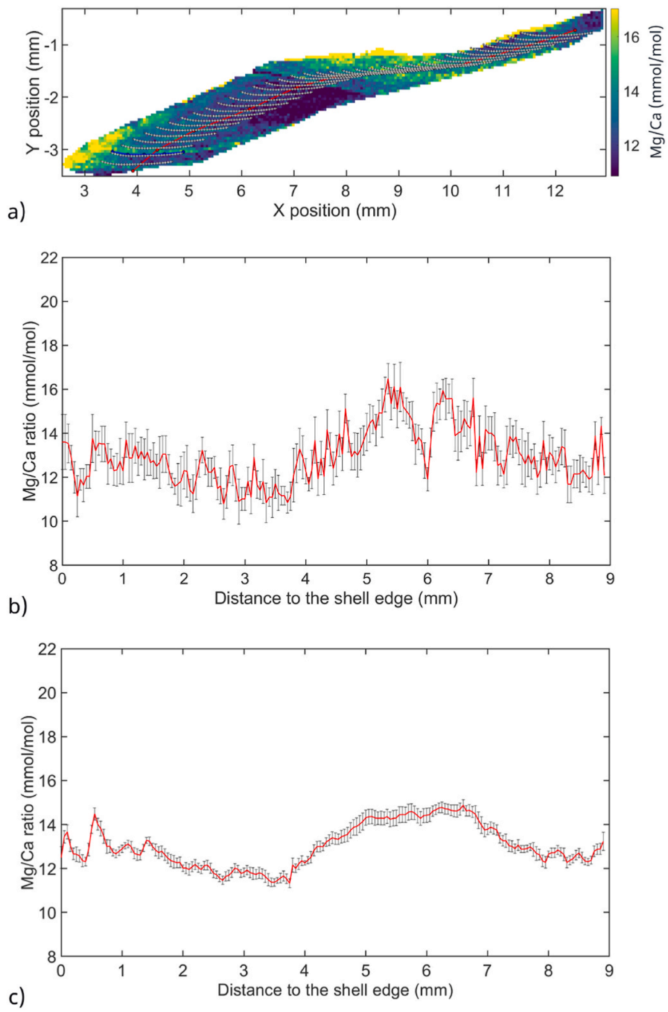

Fig. 14. (a) Mg/Ca 2D map of archaeological specimen TOR.13C.9. PV; (b) Mg/Ca profile of TOR.13C.9. PV using a single linear trajectory; (c) Mg/Ca profile of TOR.13C.9. PV using virtual sampling.

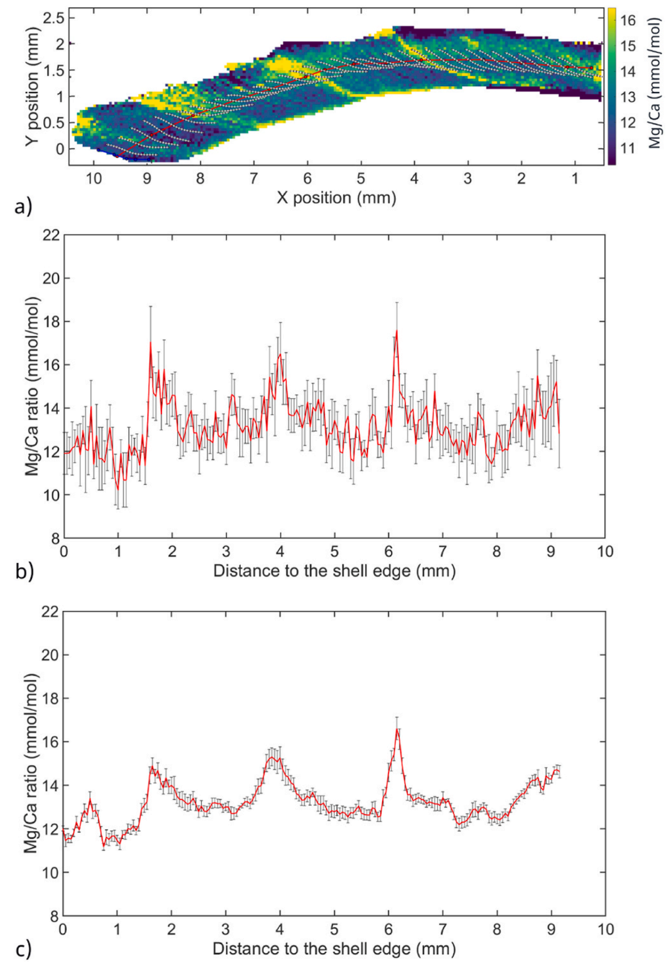

Fig. 15. (a) Mg/Ca 2D map of specimen TOR.19.3. PV; (b) Mg/Ca profile of TOR.19.3. PV using a single linear trajectory; (c) Mg/Ca profile of TOR.19.3. PV using virtual sampling.

Materials. It can be appreciated how in all the cases the VS sequence is clearly less noisy than the associated standard sequence, allowing a better interpretation of the data. For example, the use of VS presented in Fig. 15(c) (specimen TOR.19.3. PV) clearly enables the identification of 4 summer cycles at $x \approx 0.5$, 2, 4 and 6 mm, apart from a summer cycle observed on the far right of the 2D map of Fig. 15(a).

To estimate the seasons of capture for the archaeological specimens, the quartiles method proposed by Mannino et al. (2003, 2007) for $\delta^{18}O$ values obtained from marine shells, and successfully applied in different studies (Colonese et al., 2009, 2018; García-Escárzaga et al., 2019; 2024a, 2024b; Prendergast et al., 2016) was used. Basically, the intra-annual Mg/Ca ratio range of the stratigraphic unit is divided into four quartiles, each approximately corresponding to a season. The upper quartile reflects warmer conditions (i.e., summer), while the lowest quartile indicates cooler conditions (i.e., winter). Mg/Ca ratio values at the shell edge within the highest or lowest quartiles suggest the mollusc was collected during summer or winter, respectively. The middle quartiles represent transitional periods (i.e., autumn and spring). If the Mg/Ca values associated with the shell edge fall into these middle quartiles, the season of collection can be determined by considering the Mg/Ca trend before the mollusc's death. An increase in values would suggest spring, while a decrease would indicate autumn.

Table 5 shows a comparative analysis of the estimation of the seasons of collection of the *P. vulgata* archaeological specimens from El Toral III cave. Using the VS sequence of Fig. 15 associated with the specimen TOR.13C.9. PV, it can be concluded that the collection was carried out in autumn or spring, as the Mg/Ca values at the shell edge are assigned to the middle quartiles. As a descending trend is appreciated, a collection in autumn is established. The use of the $\delta^{18}O$ values produce the same estimation (data regarding the $\delta^{18}O$ values of these specimens can be found in Arniz-Mateos (2024)). Applying the same methodology to the Mg/Ca VS sequences of the other six *P. vulgata* archaeological specimens shown in Fig. 14 and Figures S.7 to S.10, the seasons of collection indicated in Table 5 are estimated. It can be observed how there is a reasonably good agreement in the estimations provided by the VS sequences and the $\delta^{18}O$ values.

A similar analysis to the one already discussed for Fig. 13 is shown in Fig. 16, in this case applied to archaeological specimens TOR.17.3. PV and TOR.22.3. PV. The estimation of the maximum and minimum values of the Mg/Ca ratio along all the growth lines is indicated by the grey bands of Fig. 16(a) and (b). In both cases the low Mg/Ca ratios and the low dispersion of the maximum and minimum concentration values appears to be consistent with a collection season in the fall/winter.

5. Conclusions

In this paper we have presented a new proposal, the virtual sampling technique, to improve the results derived from the application of LIBS to estimate the season of collection of limpet shells via their elemental analysis. Traditionally, 1D linear LIBS scans are performed through the growth axis of the shell surface, generating a profile with the evolution

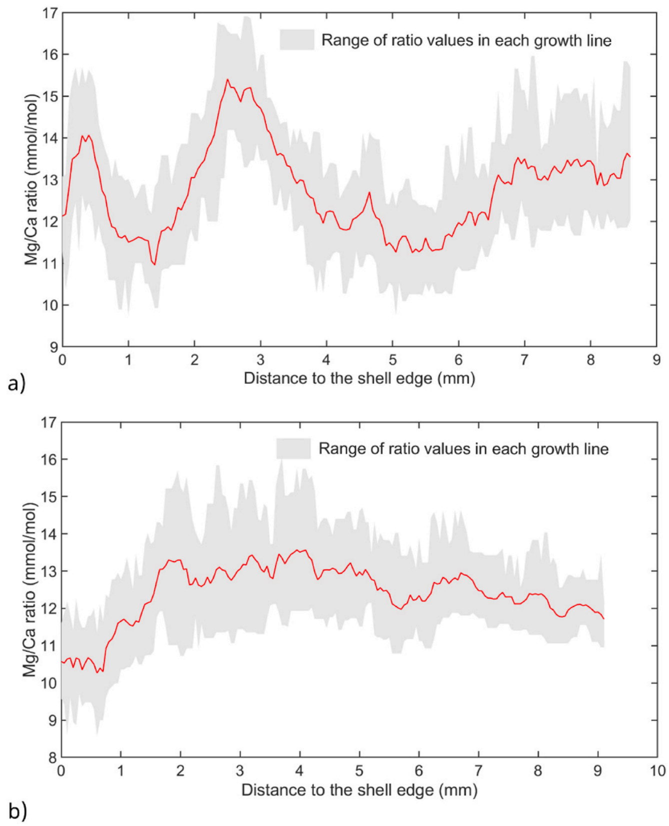

Fig. 16. VS technique and estimation of the maximum and minimum values of the Mg/Ca ratio for each growth line considered in the process: (a) analysis of TOR.17.3. PV; (b) analysis of TOR.22.3. PV.

Table 4
Estimation of season of collection by means of VS method of *P. vulgata* limpets collected in Langre between November 2011 and August 2012.

Specimen	Date of collection	Estimation via Virtual Sampling sequences	Estimation via analysis of 2D maps
LAN96	Autum	Autumn	Unclear seasonal cycle
LAN98	Autum	Autumn	Unclear seasonal cycle
LAN100	Autum	Autumn	Autumn/Winter
LAN105	Autum	Autumn	Autumn
LAN109	Autum	Autumn	Unclear seasonal cycle
LAN122	Autum	Summer	Unclear seasonal cycles
LAN176	Winter	Winter	Autumn/Winter
LAN177	Winter	Winter	Winter
LAN178	Winter	Winter	Winter
LAN182	Winter	Winter	Winter
LAN183	Winter	Winter	Winter/Spring
LAN184	Winter	Summer	Summer
LAN229	Spring	Unclear seasonal cycles	Unclear seasonal cycles
LAN230	Spring	Unclear seasonal cycles	Unclear seasonal cycles
LAN231	Spring	Spring	Unclear seasonal cycles
LAN235	Spring	Spring	Unclear seasonal cycles
LAN236	Spring	Unclear seasonal cycles	Unclear seasonal cycles
LAN237	Spring	Unclear seasonal cycles	Unclear seasonal cycles
LAN254	Summer	Summer	Summer/Autumn
LAN255	Summer	Summer	Summer/Autumn
LAN256	Summer	Summer	Summer
LAN258	Summer	Spring	Summer/Spring
LAN259	Summer	Summer	Summer
LAN261	Summer	Spring	Spring

Table 5
Estimation of season of collection by means of VS method and $\delta^{18}O$ ratio series of *P. vulgata* archaeological specimens collected in El Toral III cave.

Specimen	Estimation via Virtual Sampling sequences	Estimation via $\delta^{18}O$ values
TOR.13C.9. PV	Autumn	Autumn
TOR.22.3.PV	Winter	Autumn
TOR.19.3.PV	Spring	Spring
TOR.21.3.PV	Winter/Spring	Winter/Spring
TOR.20.5.PV	Winter	Autumn
TOR.17.3.PV	Autumn	Autumn

of the Mg/Ca ratio following that path. Given the known relationship between the Mg/Ca ratio and the environmental conditions surrounding the limpet, in particular the seawater temperature, the analysis of the Mg/Ca profile may allow the estimation of the season of collection. However, several constraints limit the quality of the obtained profile, such as the spatial resolution (that may give rise to very noisy profiles), the selection of the linear path, the presence of artefacts in some regions of the shell (particularly close to the shell edge) or the intrinsic growth behaviour of the limpets. The virtual sampling technique offers improved results of the Mg/Ca profiles by using 2D Mg/Ca maps of the shell section. The key to this technique lies in the use of the elemental information stored in the growth lines of the shell. In this way, after the definition of the linear trajectory going through the centre of the m+2 calcite, the designed algorithm is based on using a varying shape of the growth lines along the growth axis of the shell. As these growth lines are supposed to be isochronous, averaged Mg/Ca ratio values are obtained for each one. As it has been demonstrated, the VS algorithm remarkably improves the 1D Mg/Ca profiles, reducing the noise and allowing better detection of the changes and the associated cyclicity. Twenty-four specimens of *P. vulgata* shells, collected through the four seasons of the year, have been analysed, and the results delivered by the implementation of the VS algorithm and the traditional 1D linear trajectory have been compared to demonstrate the feasibility of this proposal. The study has been completed with the analysis of six archaeological specimens of *P. vulgata* from El Toral III cave, that confirms the improvement in the quality of the Mg/Ca sequence.

Regarding the estimation of the season of collection and the results presented in Tables 4 and 5, the accuracy rate in estimating the season of collection is around 66%. This confirms that, even when the measurement uncertainty is reduced using the VS approach, Mg/Ca ratios are not a reliable proxy in all specimens of *P. vulgata*. This is in line with the mixed results of elemental ratios found in studies of this and other mollusc species. However, this approach will allow future studies to focus on biological and environmental factors influencing the Mg/Ca ratios, improving the reliability of data interpretation and aiding to a better understanding of the potential and limitations of using elemental ratios for archaeological and paleoenvironmental reconstruction.

Future works should consider the possibility of achieving a better spatial resolution in the LIBS scanning to improve the analysis. An alternative method based on direct interpretation of the 2D maps via image processing techniques should also be considered, and special attention should be given to the study of more contemporary specimens of *P. vulgata*, where efforts can be made to find explanations for the issues encountered in this study with the modern specimens collected in the spring season. Different limpet species and archaeological specimens should also be studied in future works, including comparison with results provided by oxygen isotope ratio values, as well as the application of the proposed method to enable the estimation of the age of the specimens under analysis. The use of dynamic time warping algorithms to improve the alignment between the time series of the Mg/Ca ratios and the analysis via oxygen isotope ratios should be also explored, as it has offered interesting results in terms of the estimation of the season of collection of modern specimens of different limpet species in a recent study (Hausmann et al., 2024). We expect that the long-standing debate about the reliability of elemental ratios in different species could be settled by robust statistical analysis with many specimens, enabled by the convenience, speed and low cost of the LIBS technique.

CRediT authorship contribution statement

Jesús Mirapeix: Writing – original draft, Visualization, Methodology, Formal analysis. **Rosa Arniz-Mateos:** Writing – review & editing, Validation, Resources, Investigation, Formal analysis. **Asier García-Escárzaga:** Writing – review & editing, Validation, Resources, Investigation, Formal analysis. **Igor Gutierrez-Zugasti:** Supervision, Funding acquisition, Conceptualization. **José Miguel López-Higuera:** Project administration, Funding acquisition. **Adolfo Cobo:** Writing – review & editing, Software, Methodology, Funding acquisition, Data curation, Conceptualization.

Declaration of competing interest

The authors declare that they have no known competing financial interests or personal relationships that could have appeared to influence the work reported in this paper.

Acknowledgements

This research was supported by grants PID 2021-124059NB-I00, PID 2022-138350OA-I00 and PID 2022-137269OB-C2, funded by MICIU/AEI/10.13039/501100011033/and ERDF "A way of making Europe", EU; AGE was funded by the Catalonia Postdoctoral Programme through a Beatriu de Pinós fellowship (2020_BP_00240) and he is currently working in the framework of a Marie Skłodowska Curie Action – Postdoctoral Fellowship (101064225-NEARCOAST, https://doi.org/10.3030/101064225), funded by the European Commission. RAM was supported by a predoctoral grant "Concepción Arenal" (grant number: 2019-8461) in the University of Cantabria during the development of this research and she is currently working with a Postdoctoral Fellowship at the Emmy-Noether-Group SEAFRONT in LEIZA.

Appendix A. Supplementary data

Supplementary data to this article can be found online at https://doi.org/10.1016/j.jas.2024.106123.

References

Andrus, C.F.T., 2011. Shell midden sclerochronology. Quat. Sci. Rev. 30 (21–22), 2892–2905.

Arniz-Mateos, R., 2024. Procesos de intensificación en la explotación de recursos marinos durante el Mesolítico en la costa cantábrica: cambios diacrónicos y causas. Universidad de Cantabria, Santander. Unpublished PhD. Dissertation.

Arniz-Mateos, R., García-Escárzaga, A., Fernandes, R., González-Morales, M.R., Gutiérrez-Zugasti, I., 2024. Living in the shore: changes in coastal resource intensification during the Mesolithic in northern Iberia. Archaeological and Anthropological Sciences 16 (5), 1–17.

Blackmore, D.T., 1969. Studies of Patella vulgata LI Growth, reproduction and zonal distribution. J. Exp. Mar. Biol. Ecol. 3 (2), 200–213.

Bougeois, L., de Rafélis, M., Reichart, G.J., de Nooijer, L., Dupont-Nivet, G., 2015. Using Mg/Ca on oyster shells as paleoclimatic proxy, example from the Paleogene of Central Asia. In: EGU *General Assembly Conference* Abstracts, p. 493.

Branch, G.M., 1981. The biology of limpets: physical factors, energy flow, and ecological interactions. Oceanogr. Mar. Biol. Annu. Rev. 19, 235–380.

Brosset, C., Höche, N., Witbaard, R., Nishida, K., Shirai, K., Mertz-Kraus, R., Schöne, B.R., 2023. Sr/Ca in shells of laboratory-grown bivalves (Arctica islandica) serves as a proxy for water temperature–implications for (paleo) environmental research. Front. Mar. Sci. 10, 1279164.

Ciucci, A., Corsi, M., Palleschi, V., Rastelli, S., Salvetti, A., Tognoni, E., 1999. New procedure for quantitative elemental analysis by laser-induced plasma spectroscopy. Appl. Spectrosc. 53 (8), 960–964.

Cobo, A., García-Escárzaga, A., Gutiérrez-Zugasti, I., Setién, J., González-Morales, M.R., López-Higuera, J.M., 2017. Automated measurement of magnesium/calcium ratios in gastropod shells using laser-induced breakdown spectroscopy for paleoclimatic applications. Appl. Spectrosc. 71 (4), 591–599.

Colonese, A.C., Troelstra, S., Ziveri, P., Martini, F., Vetro, D.L., Tommasini, S., 2009. Mesolithic shellfish exploitation in SW Italy: seasonal evidence from the oxygen isotopic composition of Osilinus turbinatus shells. J. Archaeol. Sci. 36 (9), 1935–1944.

Colonese, A.C., Mannino, M.A., Mayer, D.B.Y., Fa, D.A., Finlayson, J.C., Lubell, D., Stiner, M.C., 2011. Marine mollusc exploitation in Mediterranean Prehistory: an overview. Quat. Int. 239 (1–2), 86–103.

Colonese, A.C., Vetro, D.L., Landini, W., Di Giuseppe, Z., Hausmann, N., Demarchi, B., et al., 2018. Late pleistocene-holocene coastal adaptation in central mediterranean: snapshots from grotta d'Oriente (NW sicily). Quat. Int. 493, 114–126.

Cortés-Sánchez, M., Simón-Vallejo, M.D., Jiménez-Espejo, F.J., Francisco, M.D.C.L., Vera-Peláez, J.L., González, A.M., Morales-Muniz, A., 2019. Shellfish collection on the westernmost Mediterranean, Bajondillo cave (~ 160-35 cal kyr BP): a case of behavioral convergence? Quat. Sci. Rev. 217, 284–296.

Crisp, D.J., 1965. Observations on the effect of climate and weather on marine communities. In: Johnson, C.G., Smith, L.P. (Eds.), The Biological Significance of Climatic Changes in Britain. Elsevier, New York, pp. 63–77.

Durham, S.R., Gillikin, D.P., Goodwin, D.H., Dietl, G.P., 2017. Rapid determination of oyster lifespans and growth rates using LA-ICP-MS line scans of shell Mg/Ca ratios. Palaeogeogr. Palaeoclimatol. Palaeoecol. 485, 201–209.

Ekaratne, S.U.K., Crisp, D.J., 1984. Seasonal growth studies of intertidal gastropods from shell micro-growth band measurements, including a comparison with alternative methods. J. Mar. Biol. Assoc. U. K. 64 (1), 183–210.

Fenger, T., Surge, D., Schöne, B., Milner, N., 2007. Sclerochronology and geochemical variation in limpet shells (Patella vulgata): a new archive to reconstruct coastal sea surface temperature. G-cubed 8 (7).

Ferguson, J.E., Henderson, G.M., Fa, D.A., Finlayson, J.C., Charnley, N.R., 2011. Increased seasonality in the Western Mediterranean during the last glacial from limpet shell geochemistry. Earth Planet Sci. Lett. 308 (3–4), 325–333.

Flores, C., Broitman, B.R., 2021. Nearshore paleoceanogaphic conditions through the holocene: shell carbonate from archaeological sites of the atacama desert coast. Palaeogeogr. Palaeoclimatol. Palaeoecol. 562, 110090.

Freitas, P., Clarke, L.J., Kennedy, H., Richardson, C., Abrantes, F., 2005. Mg/Ca, Sr/Ca, and stable-isotope (δ18O and δ13C) ratio profiles from the fan mussel Pinna nobilis: seasonal records and temperature relationships. G-cubed 6 (4).

Freitas, P.S., Clarke, L.J., Kennedy, H., Richardson, C.A., 2012. The potential of combined Mg/Ca and δ18O measurements within the shell of the bivalve Pecten maximus to estimate seawater δ18O composition. Chem. Geol. 291, 286–293.

García-Escárzaga, A., Moncayo, S., Gutiérrez-Zugasti, I., González-Morales, M.R., Martín-Chivelet, J., Cáceres, J.O., 2015. Mg/Ca ratios measured by laser induced breakdown spectroscopy (LIBS): a new approach to decipher environmental conditions. J. Anal. Atomic Spectrom. 30 (9), 1913–1919.

García-Escárzaga, A., Clarke, L.J., Gutiérrez-Zugasti, I., González-Morales, M.R., Martinez, M., López-Higuera, J.M., Cobo, A., 2018. Mg/Ca profiles within archaeological mollusc (Patella vulgata) shells: laser-induced breakdown spectroscopy compared to inductively coupled plasma-optical emission spectrometry. Spectrochim. Acta B Atom Spectrosc. 148, 8–15.

García-Escárzaga, A., Gutiérrez-Zugasti, I., Cobo, A., Cuenca-Solana, D., Martín-Chivelet, J., Roberts, P., González-Morales, M.R., 2019. Stable oxygen isotope analysis of Phorcus lineatus (da Costa, 1778) as a proxy for foraging seasonality during the Mesolithic in northern Iberia. Archaeological and Anthropological Sciences 11, 5631–5644.

García-Escárzaga, A., Gutiérrez-Zugasti, I., González-Morales, M.R., Arrizabalaga, A., Zech, J., Roberts, P., 2020. Shell sclerochronology and stable oxygen isotope ratios from the limpet Patella depressa Pennant, 1777: implications for palaeoclimate reconstruction and archaeology in northern Spain. Palaeogeogr. Palaeoclimatol. Palaeoecol. 560, 110023.

García-Escárzaga, A., Martínez-Minchero, M., Cobo, A., Gutiérrez-Zugasti, I., Arrizabalaga, A., Roberts, P., 2021. Using mg/ca ratios from the limpet patella depressa pennant, 1777 measured by laser-induced breakdown spectroscopy (LIBS) to reconstruct paleoclimate. Appl. Sci. 11 (7), 2959.

García-Escárzaga, A., Gutiérrez-Zugasti, I., Marín-Arroyo, A.B., Fernandes, R., Núñez de la Fuente, S., Cuenca-Solana, D., Roberts, P., 2022. Human forager response to abrupt climate change at 8.2 ka on the Atlantic coast of Europe. Sci. Rep. 12 (1), 6481.

García-Escárzaga, A., Gutiérrez-Zugasti, I., Arniz-Mateos, R., Cuenca-Solana, D., González-Morales, M.R., Ilgner, J., et al., 2024a. Seasonal exploitation of intertidal resources at El Mazo (N Iberia) reveals optimized human subsistence strategies during the Mesolithic in Atlantic Europe. Archaeological and Anthropological Sciences 16 (5), 1–16.

García-Escárzaga, A., Cantillo-Duarte, J.J., Milano, S., Arniz-Mateos, R., Gutiérrez-Zugasti, I., González-Ortegón, E., Corona-Borrego, J.M., Ramos-Muñoz, J., Colonese, A.C., Vijande-Vila, E., 2024b. Marine resource exploitation and human settlement patterns during the Neolithic in SW Europe: stable oxygen isotope analyses (δ18O) on Phorcus lineatus (da Costa, 1778) from Campo de Hockey (San Fernando, Cádiz, Spain). Archaeological and Anthropological Sciences 16 (3), 38.

Griem, H.R., 1963. Validity of local thermal equilibrium in plasma spectroscopy. Phys. Rev. 131 (3), 1170.

Grossman, E.L., Ku, T.L., 1986. Oxygen and carbon isotope fractionation in biogenic aragonite: temperature effects. Chem. Geol. Isot. Geosci. 59, 59–74.

Gutiérrez-Zugasti, I., Andersen, S.H., Araújo, A.C., Dupont, C., Milner, N., Monge-Soares, A.M., 2011. Shell midden research in Atlantic Europe: state of the art, research problems and perspectives for the future. Quat. Int. 239 (1–2), 70–85.

Gutiérrez-Zugasti, I., García-Escárzaga, A., Martín-Chivelet, J., González-Morales, M.R., 2015. Determination of sea surface temperatures using oxygen isotope ratios from

Phorcus lineatus (Da Costa, 1778) in northern Spain: implications for paleoclimate and archaeological studies. Holocene 25 (6), 1002–1014.
Hausmann, N., Meredith-Williams, M., 2017. Exploring accumulation rates of shelldeposits through seasonality data. J. Archaeol. Method Theor 24 (3), 776–795.
Hausmann, N., Siozos, P., Lemonis, A., Colonese, A.C., Robson, H.K., Anglos, D., 2017. Elemental mapping of Mg/Ca intensity ratios in marine mollusc shells using laser-induced breakdown spectroscopy. J. Anal. Atomic Spectrom. 32 (8), 1467–1472.
Hausmann, N., Prendergast, A.L., Lemonis, A., Zech, J., Roberts, P., Siozos, P., Anglos, D., 2019. Extensive elemental mapping unlocks Mg/Ca ratios as climate proxy in seasonal records of Mediterranean limpets. Sci. Rep. 9 (1), 3698.
Hausmann, N., Theodoraki, D., Piñon, V., Siozos, P., Lemonis, A., Anglos, D., 2023. Applying laser induced breakdown spectroscopy (LIBS) and elemental imaging on marine shells for archaeological and environmental research. Sci. Rep. 13 (1), 19812.
Hausmann, N., Surge, D., i Godino, I.B., 2024. Confirmation of Mg/Ca ratios as palaeothermometers in Atlantic limpet shells. Palaeogeogr. Palaeoclimatol. Palaeoecol., 112538
Jackson, D., Méndez, C., Aspillaga, E., 2012. Human remains directly dated to the Pleistocene-Holocene transition support a marine diet for early settlers of the Pacific coast of Chile. J. I. Coast Archaeol. 7 (3), 363–377.
Kramida, A., Ralchenko, Yu, Reader, J., NIST ASD Team, 2023. NIST Atomic Spectra Database. National Institute of Standards and Technology, Gaithersburg, MD [Online]. Available:, version 5.11. https://physics.nist.gov/asd. (Accessed 24 July 2024).
Leng, M.J., Lewis, J.P., 2016. Oxygen isotopes in Molluscan shell: applications in environmental archaeology. Environ. Archaeol. 21 (3), 295–306.
Lewis, J.P., Ryves, D.B., Rasmussen, P., Olsen, J., Van der Sluis, L.G., Reimer, P.J., et al., 2020. Marine resource abundance drove pre-agricultural population increase in Stone Age Scandinavia. Nat. Commun. 11 (1), 2006.
Little, C., Trowbridge, C.D., Pilling, G.M., Stirling, P., Morritt, D., Williams, G.A., 2017. Long-term fluctuations in intertidal communities in an Irish sea-lough: limpet-fucoid cycles. Estuar. Coast Shelf Sci. 196, 70–82.
Lombardo, U., Szabo, K., Capriles, J.M., May, J.H., Amelung, W., Hutterer, R., et al., 2013. Early and middle Holocene hunter-gatherer occupations in Western Amazonia: the hidden shell middens. PLoS One 8 (8), e72746.
Mannino, M.A., Spiro, B.F., Thomas, K.D., 2003. Sampling shells for seasonality: oxygen isotope analysis on shell carbonates of the inter-tidal gastropod Monodonta lineata (da Costa) from populations across its modern range and from a Mesolithic site in southern Britain. J. Archaeol. Sci. 30 (6), 667–679.
Mannino, M.A., Thomas, K.D., 2007. Determining the season of collection of inter-tidal gastropods from δ18O analysis of shell carbonates: modern analogue data and "internal analysis" of data from archaeological shells. In: Milner, N., Craig, O.E., Bailey, G.N. (Eds.), Shells Middens in Atlantic Europe. Oxbow Books, Oxford, pp. 111–122.
Mannino, M.A., Thomas, K.D., Leng, M.J., Di Salvo, R., Richards, M.P., 2011. Stuck to the shore? Investigating prehistoric hunter-gatherer subsistence, mobility and territoriality in a Mediterranean coastal landscape through isotope analyses on marine mollusc shell carbonates and human bone collagen. Quat. Int. 244 (1), 88–104.
Marali, S., Schöne, B.R., Mertz-Kraus, R., Griffin, S.M., Wanamaker, Jr A.D., Butler, P.G., et al., 2017. Reproducibility of trace element time-series (Na/Ca, Mg/Ca, Mn/Ca, Sr/Ca, and Ba/Ca) within and between specimens of the bivalve Arctica islandica–A LA-ICP-MS line scan study. Palaeogeogr. Palaeoclimatol. Palaeoecol. 484, 109–128.
Marotta, A., 1994. Determination of axial thermal plasma temperatures without Abel inversion. Journal of Physics D. Appl. Phys. 27 (2), 268.
Martínez-Minchero, M., Cobo, A., Méndez-Vicente, A., Pisonero, J., Bordel, N., Gutiérrez-Zugasti, I., et al., 2023. Comparison of Mg/Ca concentration series from Patella depressa limpet shells using CF-LIBS and LA-ICP-MS. Talanta 251, 123757.
MacClintock, C., 1967. Shell structure of patelloid and bellerophontoid gastropods (Mollusca). Peabody Museum of Natural History, Yale University, Bulletin, 22, 140.
Poulain, C., Gillikin, D.P., Thebault, J., Munaron, J.-M., Bohn, M., Robert, R., Paulet, Y.-M., Lorrain, A., 2015. An evaluation of Mg/Ca, Sr/Ca, and Ba/Ca ratios as environmental proxies in aragonite bivalve shells. Chem. Geol. 396, 42–50.
Prendergast, A.L., Stevens, R.E., O'connell, T.C., Fadlalak, A., Touati, M., Al-Mzeine, A., et al., 2016. Changing patterns of eastern Mediterranean shellfish exploitation in the Late Glacial and Early Holocene: oxygen isotope evidence from gastropod in Epipaleolithic to Neolithic human occupation layers at the Haua Fteah cave, Libya. Quat. Int. 407, 80–93.
Prendergast, A.L., Versteegh, E.A.A., Schöne, B.R., 2017. New research on the development of high-resolution palaeoenvironmental proxies from geochemical properties of biogenic carbonates. Palaeogeogr. Palaeoclimatol. Palaeoecol. 484, 1–6.
Ramos-Muñoz, J., Cantillo-Duarte, J.J., Bernal-Casasola, D., Barrena-Tocino, A., Domínguez-Bella, S., Vijande-Vila, E., et al., 2016. Early use of marine resources by Middle/Upper Pleistocene human societies: the case of Benzú rockshelter (northern Africa). Quat. Int. 407, 6–15.
Roberts, P., Prendergast, M.E., Janzen, A., Shipton, C., Blinkhorn, J., Zech, J., et al., 2020. Late Pleistocene to Holocene human palaeoecology in the tropical environments of coastal eastern Africa. Palaeogeogr. Palaeoclimatol. Palaeoecol. 537, 109438.
Schöne, B.R., 2008. The curse of physiology—challenges and opportunities in the interpretation of geochemical data from mollusk shells. Geo Mar. Lett. 28, 269–285.
Schöne, B.R., Zhang, Z., Radermacher, P., Thébault, J., Jacob, D.E., Nunn, E.V., Maurer, A.F., 2011. Sr/Ca and Mg/Ca ratios of ontogenetically old, long-lived bivalve shells (Arctica islandica) and their function as paleotemperature proxies. Palaeogeogr. Palaeoclimatol. Palaeoecol. 302 (1–2), 52–64.
Surge, D., Wang, T., Gutiérrez-Zugasti, I., Kelley, P.H., 2013. Isotope sclerochronology and season of annual growth line formation in limpet shells (Patella vulgata) from warm-and cold-temperate zones in the eastern North Atlantic. Palaios 28 (6), 386–393.
Thomas, K.D., 2015. Molluscs emergent, Part I: themes and trends in the scientific investigation of mollusc shells as resources for archaeological research. J. Archaeol. Sci. 56, 133–140.
Wanamaker, Jr. A.D., Kreutz, K.J., Wilson, T., Borns, Jr. H.W., Introne, D.S., Feindel, S., 2008. Experimentally determined Mg/Ca and Sr/Ca ratios in juvenile bivalve calcite for Mytilus edulis: implications for paleotemperature reconstructions. Geo Mar. Lett. 28 (5–6), 359–368.
Wanamaker, A.D., Kreutz, K.J., Schöne, B.R., Pettigrew, N., Borns, H.W., Introne, D.S., et al., 2008b. Coupled North Atlantic slope water forcing on Gulf of Maine temperatures over the past millennium. Clim. Dynam. 31, 183–194.
Winefordner, J.D., Gornushkin, I.B., Correll, T., Gibb, E., Smith, B.W., Omenetto, N., 2004. Comparing several atomic spectrometric methods to the super stars: special emphasis on laser induced breakdown spectrometry, LIBS, a future super star. J. Anal. Atomic Spectrom. 19 (9), 1061–1083.